CEAS EuroGNC 2022
"Conference on Guidance, Navigation and Control"
3-5 May 2022 @ Technische Universität Berlin, Germany

Passivity Based Cross-Track Control of a Fixed-Wing Aircraft

Jean-Michel Fahmi   Graduate Student, Virginia Tech, Kevin T. Crofton Department of Aerospace and Ocean Engineering, 24060, Blacksburg, VA, USA. fahmi@vt.edu

Craig A. Woolsey   Professor, Virginia Tech, Kevin T. Crofton Department of Aerospace and Ocean Engineering, 24060, Blacksburg, VA, USA. cwoolsey@vt.edu

ABSTRACT

The paper addresses the time-varying directional stabilization problem for a small, fixed-wing unmanned aircraft with using nonlinear feedback control of the thrust and the three control moments about the roll, pitch, and yaw axes. The control law makes use of the passivity property gained by modeling the aircraft as a port-Hamiltonian system. The static state feedback control law is designed following an energy-shaping approach to leverage the open-loop system's port-Hamiltonian structure in order to construct a control Lyapunov function. The proof of stability requires only basic assumptions about the aerodynamic forces and moments, rather than explicit formulas, and it ensures asymptotic stability of the desired flight condition within a sizeable region of attraction. The directional stabilization algorithm is then extended by including a line-of-sight guidance law and varying the direction as a function of position relative to a desired path, rather than as a function of time. The resulting control law and the associated proof of stability follow similarly to that of the time-varying directional stabilization problem.

1 Introduction

Recent advancements in fixed-wing unmanned aircraft systems (UAS) technology have resulted in more agile aircraft, such as the Kratos XQ-58 Valkyrie and Boeing Airpower Teaming System, which are capable of aggressive maneuvering. Such aircraft require advanced control laws to take full advantage of their agility. Conventional approaches to flight control of fixed-wing aircraft rely on linearizing the vehicle dynamics about an equilibrium motion, such as wings-level flight at constant speed. The utility of control schemes, such as linear-quadratic or H_∞ control, that rely on a small perturbation model is limited to a neighborhood of the nominal flight condition. One can develop a family of controllers that are parameterized by desired speed, climb angle, turn rate, etc., but the performance and stability of the resulting closed-loop system will generally depend on the rate of parameter variation.

To obtain effective closed-loop performance with stability guarantees over a larger operating envelope, one may instead consider nonlinear control design methods such as dynamic inversion [1–3] or adaptive control [4–6]. Dynamic inversion, or feedback linearization, requires a well-characterized model of the nonlinear dynamics. Such a model may be impractical to obtain over the full flight envelope, particularly for an aircraft whose configuration and inertial parameters vary substantially between flights. Model reference adaptive control and adaptive backstepping can accommodate a variety of uncertainties,

including uncertain nonlinearities, assuming the system satisfies certain structural conditions. The resulting dynamic state feedback controllers are often computationally sophisticated, however, which can limit their utility for low-cost platforms such as small unmanned aircraft.

The design proposed in this paper is based on modeling the aircraft as a port-Hamiltonian system (PHS) [7], an extension of Hamiltonian systems in classical mechanics to systems with inputs, outputs, and dissipation. PHS are characterized by an energy-like scalar function, which often is the total system energy, along with a pair of matrix-valued functions that describe how this energy is distributed and dissipated. Modeling the system as a PHS facilitates nonlinear, energy-based control design and allows using established energy-shaping techniques for PHS [8], such as interconnection and damping assignment, passivity-based control (IDA-PBC) [9]. Passivity-based control (PBC) has proven to be effective in various applications such as the control of electric motors [10] and quadrotors [11–16].

Of the many mechanical system applications of PBC described in the current literature, perhaps the closest to the proposed application of fixed-wing aircraft flight control is the use of PBC to control unmanned underwater vehicles (UUVs). Woolsey and Techy [17] developed a cross-track control law for a slender, underactuated UUV using potential energy shaping. Fahmi and Woolsey [18] adapted this notion of potential energy shaping for directional stabilization of a fixed-wing aircraft. The closed-loop performance exhibited undesirable excursions in the aerodynamic angles, however, particularly in sideslip. In a different approach to energy shaping, Valentinis *et al* [19] developed a feedback controller for a slender, underactuated UUV by shaping the target dynamics and suppressing the influence of un-actuated degrees of freedom. In [20], Valentinis *et al* expanded the scope of control design to include precision guidance along a helical trajectory. More recently, Valentinis and Woolsey [21] developed a passivity-based controller for a non-neutrally buoyant, underactuated submarine in ascending motion.

With the exception of [21], the studies mentioned above ignore the force of gravity, which is balanced by the hydrostatic force for a neutrally buoyant vehicle. While hydrodynamic forces such as lift and drag certainly affect underwater vehicle motion, these forces can be considered perturbations to the nominal state of motion in which the vehicle proceeds at constant speed with zero lift. The task of the control system is to reject these and other perturbations. In contrast, fixed-wing aircraft rely on aerodynamic lift to counter gravity in steady flight and to execute maneuvers. Fahmi and Woolsey [22] focused on stabilizing the aircraft velocity by exploiting some remarkable properties of the aerodynamic force when expressed in a port-Hamiltonian framework. The approach to control design was inspired by the canonical transformation approach proposed by Fujimoto *et al* [23]. However, the resulting control system's rate of convergence to the desired motion, a prescribed inertial velocity, is too slow for acceptable cross-track control performance. This paper extends the work presented in [22] by addressing time-varying directional stabilization. The resulting control design method then allows us to address the cross-track control problem for piecewise linear path following.

2 Port-Hamiltonian Systems

The design presented in this paper extends the work presented in [22], which is based on the trajectory control design described by Fujimoto *et al* [23], which in turn relies on a general theoretical framework for under-actuated electro-mechanical systems. Similar to the IDA-PBC method described by Ortega *et al* [9], this framework can be considered a generalization of IDA-PBC for time-varying systems. A port-Hamiltonian system has the following form:

$$\dot{\boldsymbol{x}} = [\boldsymbol{J}(\boldsymbol{x}) - \boldsymbol{D}(\boldsymbol{x})] \frac{\partial \mathscr{H}}{\partial \boldsymbol{x}}^{\mathrm{T}} + \boldsymbol{g}(\boldsymbol{x})\boldsymbol{u} \tag{1}$$

$$\boldsymbol{y} = \boldsymbol{g}^{\mathrm{T}}(\boldsymbol{x}) \frac{\partial \mathscr{H}}{\partial \boldsymbol{x}}^{\mathrm{T}} \tag{2}$$

where $\boldsymbol{x}(t) \in \mathbb{R}^n$ is the state vector, the matrix $\boldsymbol{J}$ is a skew-symmmetric interconnection matrix which encapsulates the energy conserving interactions between the state variables, and $\boldsymbol{D}$ is a positive semi-definite matrix which accounts for the energy dissipating interactions. (Note that the dissipation matrix in earlier work was designated with the letter $\boldsymbol{R}$. To distinguish between dissipation and rotation matrices, though, we use the letter $\boldsymbol{D}$ for "dissipation" here instead.) The Hamiltonian $\mathscr{H} : \mathbb{R}^n \to \mathbb{R}$ accounts for the energy, physical or otherwise, that is stored within the system. The vectors $\boldsymbol{u}(t)$, $\boldsymbol{y}(t) \in \mathbb{R}^m$ are the system input and output vectors, respectively. They are conjugate in the sense that their inner product represents the power applied to the system. The system input matrix $\boldsymbol{g}(\boldsymbol{x})$ also appears in the system output, ensuring conjugacy of the input and output, as mentioned above. The port-Hamiltonian system is passive [7] with the Hamiltonian as a storage function:

$$\frac{\mathrm{d}\mathscr{H}(\boldsymbol{x})}{\mathrm{d}t} = \boldsymbol{y}^{\mathrm{T}}\boldsymbol{u} - \frac{\partial \mathscr{H}(\boldsymbol{x})}{\partial \boldsymbol{x}} \boldsymbol{D}(\boldsymbol{x}) \frac{\partial \mathscr{H}(\boldsymbol{x})}{\partial \boldsymbol{x}}^{\mathrm{T}} \le \boldsymbol{y}^{\mathrm{T}}\boldsymbol{u} \tag{3}$$

The goal of the work presented in this paper is to use the port-Hamiltonian system structure of a flight dynamic model for a fixed-wing aircraft in order to construct a nonlinear, static, state feedback control law that drives the aircraft to a desired state of motion: steady flight along a specified piecewise linear path.

3 Vehicle Motion Model

The flight dynamic model described in this section is detailed in [22]. We consider a rigid fixed-wing aircraft with three control moments in roll, pitch, and yaw and with a single control force that acts along an axis fixed in the aircraft. Let an orthonormal triad pointing north, east, and down define an "inertial enough" reference frame fixed at a point on the Earth's surface. Also, define an orthonormal triad centered at the aircraft center of mass with axes pointing toward the nose, along the right wing, and out the belly of the aircraft and let this triad define a body-fixed reference frame. Let $\boldsymbol{\omega} = [p, q, r]^{\mathrm{T}}$ represent the angular velocity of the body frame with respect to the inertial frame, but expressed in the body frame. The vector $\boldsymbol{h} = [h_1, h_2, h_2]^{\mathrm{T}} = \boldsymbol{I}\boldsymbol{\omega}$ denotes the body angular momentum, with $\boldsymbol{I}$ being the matrix of moments of inertia. The translational velocity of the aircraft with respect to the inertial frame, but expressed in the body frame, is represented by the vector $\boldsymbol{v} = [u, v, w]^{\mathrm{T}}$ and the corresponding translational momentum is $\boldsymbol{p} = [p_1, p_2, p_2]^{\mathrm{T}} = m\boldsymbol{v}$ where m is the aircraft mass. We also define the scalars $V = \|\boldsymbol{v}\|$ (the airspeed) and $P = \|\boldsymbol{p}\| = mV$. It is sometimes convenient to express the body velocity components in spherical coordinate form $(u, v, w) \to (V, \beta, \alpha)$:

$$\alpha = \arctan_4\left(\frac{w}{u}\right) \quad \text{and} \quad \beta = \arcsin\left(\frac{v}{V}\right) \tag{4}$$

where $\arctan_4$ denotes the 4-quadrant arctangent. We can use the aerodynamic angles, β and α, to define a proper rotation matrix which maps vectors from the wind frame, where the aerodynamic forces are defined, to the body frame [24]:

$$\mathbf{R}_{\mathrm{BW}}(\alpha, \beta) = e^{-\hat{\boldsymbol{e}}_2\alpha} e^{\hat{\boldsymbol{e}}_3\beta} \tag{5}$$

Here, $\boldsymbol{e}_i$ is the ith unit basis vector for $\mathbb{R}^3$ and the overhat symbol, $\hat{}$, denotes the 3×3 skew-symmetric "cross-product equivalent matrix" which satisfies the relation $\hat{\boldsymbol{a}}\boldsymbol{b} = \boldsymbol{a} \times \boldsymbol{b}$ for all $\boldsymbol{a}, \boldsymbol{b} \in \mathbb{R}^3$.

The orientation of the aircraft with respect to the inertial frame can be expressed using a common Euler angle parametrization for the rotation matrix that maps free vectors from the body frame to the inertial frame:

$$\boldsymbol{R}_{IB}(\phi, \theta, \psi) = e^{\psi\hat{\boldsymbol{e}}_3}e^{\theta\hat{\boldsymbol{e}}_2}e^{\phi\hat{\boldsymbol{e}}_1}$$

The rotational kinematic equations are well defined for this parametrization provided $\theta \neq \pm\frac{\pi}{2}$. Alternatively, one may adopt a notation similar to that used in [25] and define the *tilt* vector $\boldsymbol{\zeta} = \boldsymbol{R}_{IB}\boldsymbol{e}_3$ and the *forward* vector $\boldsymbol{\lambda} = \boldsymbol{R}_{IB}\boldsymbol{e}_1$ in order to express the attitude kinematics. This parametrization is valid provided $\boldsymbol{\zeta} = \pm\boldsymbol{e}_1$, i.e., provided that the longitudinal (roll) axis of the aircraft is not aligned with the inertial vertical axis. (This condition is equivalent to the one for the Euler angle parametrization.) With these definitions, one may write

$$\boldsymbol{R}_{IB}(\boldsymbol{\lambda}, \boldsymbol{\zeta}) = \left[\boldsymbol{\lambda}, \ \hat{\boldsymbol{\zeta}}\boldsymbol{\lambda}, \ \boldsymbol{\zeta} \right]^{\mathrm{T}} \tag{6}$$

The aircraft kinematics can then be expressed as

$$\dot{\boldsymbol{\zeta}} = \boldsymbol{\zeta} \times \boldsymbol{\omega} \tag{7}$$

$$\dot{\boldsymbol{\lambda}} = \boldsymbol{\lambda} \times \boldsymbol{\omega} \tag{8}$$

$$\dot{\boldsymbol{q}} = \boldsymbol{R}_{IB}\boldsymbol{v} \tag{9}$$

The dynamic equations for flight in still air are

$$\dot{\boldsymbol{h}} = \boldsymbol{h} \times \boldsymbol{\omega} + \boldsymbol{\tau}_{\mathrm{a}} + \boldsymbol{\tau}_{\mathrm{c}} \tag{10}$$

$$\dot{\boldsymbol{p}} = \boldsymbol{p} \times \boldsymbol{\omega} + mg\boldsymbol{\zeta} + \boldsymbol{f}_{\mathrm{a}} + \boldsymbol{f}_{\mathrm{c}} \tag{11}$$

where $\boldsymbol{\tau}_{\mathrm{a}}$ and $\boldsymbol{\tau}_{\mathrm{c}}$ are the aerodynamic and control moments, respectively, and $\boldsymbol{f}_{\mathrm{a}}$ and $\boldsymbol{f}_{\mathrm{c}}$ are the aerodynamic and control forces. The aircraft is fully actuated in attitude but the control force acts in a fixed direction, relative to the body. We assume that thrust is aligned with the *x*-axis of the *stability frame*, which is obtained pitching the body *x*-axis down by the desired angle of attack α_{d}. Thus, $\boldsymbol{f}_{\mathrm{c}} = F_{\mathrm{c}}\boldsymbol{R}_{BW_{\mathrm{d}}}\boldsymbol{e}_1$ where $F_{\mathrm{c}} \in \mathbb{R}$ is the force magnitude and $\boldsymbol{R}_{BW_{\mathrm{d}}} = \boldsymbol{R}_{BW}(\alpha_{\mathrm{d}}, 0)$. This assumption is uncommon, as it requires that the propulsor be aligned with the nominal body velocity vector, but it overcomes an analytical impasse in the stability analysis. We compare this assumption with more common assumptions about the propulsive force in Section 6.

Instead of using explicit analytical expressions for aerodynamic effects, we adopt a general set of assumptions about them for stability analysis. Specifically, we assume the aerodynamic force and moment are governed by quasi-steady flow and depend only on the rotational and translational velocity. The aerodynamic moment has damping components which resist rotational velocity and other components which depend on the translational velocity, such as the "weathervane" moments in pitch and yaw. These velocity-dependent components of the aerodynamic moment are omitted from the model during control design and then restored by subtracting them from the final control moment obtained through the design process. A simple aerodynamic moment model that captures the primary effects of roll, pitch, and yaw damping is: $\boldsymbol{\tau}_{\mathrm{a}} = -\boldsymbol{D}_\omega(\boldsymbol{v})\boldsymbol{\omega}$, where $\boldsymbol{D}_\omega \succ 0$.

The aerodynamic force is typically expressed in wind frame components: the drag force, which opposes velocity; the lift force, which acts normal to drag and in the aircraft plane of symmetry; and the side force, which is normal to the two other components. These components are assumed to depend solely on the aerodynamic angles. In reality, small aerodynamic forces also arise in response to aircraft rotation. For example, an aircraft rotating in yaw will experience a small side force due to the vertical stabilizer. (This small force, acting about the center of gravity through a large moment arm, provides

a yaw damping moment.) We ignore these small aerodynamic forces due to rotational motion in the control design and analysis, although we retain the aerodynamic moments that they generate. These small aerodynamic forces are included in the simulation model, however.

For a given (constant) air density ρ and wing planform area S, the aerodynamic force expressed in the body reference frame can be written as:

$$f_a(v) = -\frac{1}{2}\rho S V^2 \mathbf{R}_{\mathrm{BW}}(\alpha, \beta) C(\alpha, \beta) \tag{12}$$

where $C(\alpha, \beta) = [C_D(\alpha, \beta), C_S(\alpha, \beta), C_L(\alpha, \beta)]^T$ contains the indicated nondimensional aerodynamic force coefficients. These are assumed to exhibit the following properties:

- The drag coefficient, $C_D(\alpha, \beta)$, is a positive function and even in both arguments.
- The side force coefficient, $C_S(\alpha, \beta)$, is a smooth, odd function with respect to β. It is positive (resp., negative) when when $e^{i\beta}$ lies in the first (resp., fourth) quadrant of the complex plane.[1]
- The lift coefficient, $C_L(\alpha, \beta)$, is a smooth function and nondecreasing with respect to α.

While the third condition given above allows a diminishing slope of the lift coefficient near the stall angle of attack, it prohibits the decrease in lift coefficient that occurs with increasing angle of attack beyond the stall condition. Thus, while the aerodynamic model is quite general in its representation of normal flight conditions, the subsequent analysis and results require (and help to ensure) that the aircraft operates below the stall condition.

Using the definitions of aerodynamic angles in equations (4) and (5), we can reformulate the aerodynamic forces as follows:

$$f_a(v) = -\bar{\rho} \begin{bmatrix} uVC_D - \frac{uvV}{\sqrt{u^2+w^2}}C_S - \frac{wV^2}{\sqrt{u^2+w^2}}C_L \\ vVC_D + V\sqrt{u^2+w^2}C_S \\ wVC_D - \frac{vwV}{\sqrt{u^2+w^2}}C_S + \frac{uV^2}{\sqrt{u^2+w^2}}C_L \end{bmatrix} \tag{13}$$

where $\bar{\rho} = \frac{1}{2}\rho S$ is assumed to be constant and the drag, side-force and lift coefficients depend on the velocity v. Equation (13) can be further decomposed as follows:

$$f_a(v) = \left(\widehat{J}_v - D_v\right) v \tag{14}$$

where $J_v = \frac{\bar{\rho}V}{\sqrt{u^2+w^2}}[wC_S, VC_L, -uC_S]^T$ accounts for a force orthogonal to the velocity vector (i.e., a turning force) and where the matrix $D_v = \bar{\rho}VC_D\mathbb{I} \succ 0$ accounts for the dissipation of translational kinetic energy. (The symbol $\mathbb{I}$ represents the 3×3 identity matrix.)

Let $v = [P, \beta, \alpha]$ be the vector of translational dynamic state variables, equivalent to the body velocity. The equations of motion can be rewritten as

$$\dot{v} = B R_{BW}^T \dot{p}, \tag{15}$$

where $B(P, \beta) = \mathrm{diag}\left(1, P^{-1}, (P\cos\beta)^{-1}\right)$. Let the input vector be the concatenation of the control moments and the control thrust $u = \left[\tau_c^T, F_c\right]^T$. Also, let $\eta = \left[\zeta^T, \lambda^T, q^T\right]^T$ be the configuration vector, where q denotes the position of the aircraft in inertial space. We now define the state vector $x = \left[h^T, v^T, \eta^T\right]^T$, the concatenation of configuration and momentum.

---

[1]Note that the sign of C_S is opposite the standard convention for lateral force coefficient.

As shown in [22], the dynamics (7-11) and (15) can be written in the PHS form (1-2) with

$$\mathscr{H} = \frac{1}{2}\boldsymbol{h}^{\mathrm{T}}\boldsymbol{I}^{-1}\boldsymbol{h} + \frac{P^2}{2m} - mg\boldsymbol{e}_3^{\mathrm{T}}\boldsymbol{q} \tag{16}$$

and with

$$\boldsymbol{J} = \begin{bmatrix} \hat{\boldsymbol{h}} & \boldsymbol{R}_{BW}\hat{\boldsymbol{e}}_1\boldsymbol{B} & \hat{\boldsymbol{\zeta}} & \hat{\boldsymbol{\lambda}} & 0 \\ \boldsymbol{B}\hat{\boldsymbol{e}}_1\boldsymbol{R}_{BW}^{\mathrm{T}} & \hat{\boldsymbol{J}}_v & 0 & 0 & -\boldsymbol{B}\boldsymbol{R}_{BW}^{\mathrm{T}}\boldsymbol{R}_{\mathrm{IB}}^{\mathrm{T}} \\ \hat{\boldsymbol{\zeta}} & 0 & 0 & 0 & 0 \\ \hat{\boldsymbol{\lambda}} & 0 & 0 & 0 & 0 \\ 0 & \boldsymbol{R}_{IB}\boldsymbol{R}_{BW}\boldsymbol{B} & 0 & 0 & 0 \end{bmatrix}, \quad \boldsymbol{D} = \begin{bmatrix} \boldsymbol{D}_\omega & 0 & 0 & 0 & 0 \\ 0 & \boldsymbol{D}_v & 0 & 0 & 0 \\ 0 & 0 & 0 & 0 & 0 \\ 0 & 0 & 0 & 0 & 0 \\ 0 & 0 & 0 & 0 & 0 \end{bmatrix}, \quad \boldsymbol{g} = \begin{bmatrix} \mathbb{I} & 0 \\ 0 & \boldsymbol{B}\boldsymbol{R}_{BW}^{\mathrm{T}}\boldsymbol{R}_{BW_{\mathrm{d}}}\boldsymbol{e}_1 \\ 0 & 0 \\ 0 & 0 \\ 0 & 0 \end{bmatrix} \tag{17}$$

where $\boldsymbol{J}_v = \boldsymbol{B}\boldsymbol{R}_{BW}^{\mathrm{T}}\boldsymbol{J}_v = -\frac{\bar{\rho}}{m}\left[0, \frac{C_L}{\cos\beta}, -C_s\right]^{\mathrm{T}}$ and $\boldsymbol{D}_v = \bar{\rho}VC_D\boldsymbol{e}_1\boldsymbol{e}_1^{\mathrm{T}}$. Recall that $\mathbf{R}_{\mathrm{IB}}$ depends on both $\boldsymbol{\lambda}$ and $\boldsymbol{\zeta}$ while $\boldsymbol{R}_{BW}$ depends on both α and β. Note that this PHS formulation holds for aerodynamic coefficients C_D, C_S, and C_L of any functional form. The assumptions following (12) come into play when analyzing closed-loop stability for the control law to be designed in Section 4.

4 Directional Stabilization

The procedure followed in this section follows similarly to the one detailed in [22] and is based on the work of Fujimoto *et al* [23], whose paper details a trajectory tracking control strategy where a passive error dynamic system is constracted from a port-Hamiltonian system through canonical transformation.

The goal in this section is to stabilize the aircraft's motion to non-slipping flight while following a time-varying inertial direction specified by a desired course angle, $\chi_{\mathrm{d}}(t)$, and a climb angle, $\gamma_{\mathrm{d}}(t) \neq \pm\frac{\pi}{2}$. To ensure that the aircraft does not incur any sideslip during its motion, a desired bank angle, $\mu_{\mathrm{d}}(t)$, is also prescribed. These time-varying reference signals are obtained from the cross-track error.

To avoid specifying a particular functional form of the aerodynamic force coefficient, the desired angle of attack α_{d} is specified and the corresponding desired airspeed is then determined. Specifying the angle of attack does not require knowledge of the force coefficient functions and it helps one avoid prescribing a flight condition approaches or exceeds the stall limit. Choosing a sensible nominal flight condition and then prescribing bounds on the operational envelope, by restricting motion to a sub-level set of a Lyapunov function to be developed, can ensure the aircraft does not approach the stall condition. A change in the lift force required at the desired steady state would be reflected by a change in the desired airspeed rather than the desired angle of attack.

The desired attitude is chosen to attain the desired inertial velocity provided that the desired aerodynamic angles are attained. The approach adopted in this work is to modify the aircraft's attitude to track the reference inertial velocity direction while maintaining the desired aerodynamic angles. As such, the desired attitude vectors can be expressed as $\boldsymbol{\zeta}_{\mathrm{d}} = \boldsymbol{R}_{BW_{\mathrm{d}}}\boldsymbol{R}_{\mathrm{d}}^{\mathrm{T}}\boldsymbol{e}_3$ and $\boldsymbol{\lambda}_{\mathrm{d}} = \boldsymbol{R}_{BW_{\mathrm{d}}}\boldsymbol{R}_{\mathrm{d}}^{\mathrm{T}}\boldsymbol{e}_1$, where the rotation matrix $\boldsymbol{R}_{\mathrm{d}} = e^{\chi_{\mathrm{d}}\hat{\boldsymbol{e}}_3}e^{\gamma_{\mathrm{d}}\hat{\boldsymbol{e}}_2}e^{\mu_{\mathrm{d}}\hat{\boldsymbol{e}}_1}$, parameterized by the desired course, climb, and bank angles χ_{d}, γ_{d}, and μ_{d}, respectively, is defined such that $\boldsymbol{R}_{\mathrm{d}}\boldsymbol{e}_1$ expresses the desired direction of motion in the inertial frame.

The desired angular velocity is $\boldsymbol{\omega}_{\mathrm{d}}(t) = \boldsymbol{R}_{BW_{\mathrm{d}}}\bar{\boldsymbol{\omega}}(t)$ where $\bar{\boldsymbol{\omega}}(t) = \left(\dot{\mu}_{\mathrm{d}}\boldsymbol{e}_1 + e^{-\mu_{\mathrm{d}}\hat{\boldsymbol{e}}_1}\left(\dot{\gamma}_{\mathrm{d}}\boldsymbol{e}_2 + \dot{\chi}_{\mathrm{d}}e^{-\gamma_{\mathrm{d}}\hat{\boldsymbol{e}}_2}\boldsymbol{e}_3\right)\right)$.

In this expression, the desired bank angle is chosen to counteract the effects of $\dot{\chi}_{\mathrm{d}}$ and $\dot{\gamma}_{\mathrm{d}}$ on sideslip at steady state:

$$\mu_{\mathrm{d}}(t) = \tan^{-1}\left(-\frac{V_{\mathrm{d}}\dot{\chi}_{\mathrm{d}}\cos\gamma_{\mathrm{d}}}{g\cos\gamma_{\mathrm{d}} + V_{\mathrm{d}}\dot{\gamma}_{\mathrm{d}}}\right) \tag{18}$$

The desired airspeed satisfies: $mV_{\mathrm{d}}(t)\bar{\omega}_2 - \bar{\rho}V_{\mathrm{d}}^2(t)C_{L_{\mathrm{d}}} + mg\boldsymbol{e}_3^{\mathrm{T}}\boldsymbol{R}_{BW_{\mathrm{d}}}^{\mathrm{T}}\boldsymbol{\zeta}_{\mathrm{d}} = 0$, where $\bar{\omega}_2 = \boldsymbol{e}_2^{\mathrm{T}}\bar{\boldsymbol{\omega}} = \dot{\gamma}\cos\mu + \dot{\chi}\cos\gamma\sin\mu$. Inserting equation (18) in the equation gives:

$$(\bar{\rho}C_{L_{\mathrm{d}}})^2 V_{\mathrm{d}}^4 = m^2\left(g\cos\gamma_{\mathrm{d}} + V_{\mathrm{d}}\dot{\gamma}_{\mathrm{d}}\right)^2 + \left(mV_{\mathrm{d}}\dot{\chi}_{\mathrm{d}}\cos\gamma_{\mathrm{d}}\right)^2 \tag{19}$$

While one might find an analytical solution for V_{d} from this fourth order polynomial, the expression is complicated. We instead differentiate the expression to obtain the differential equation

$$\dot{V}_{\mathrm{d}} = \frac{2m^2\left(\left(g\cos\gamma_{\mathrm{d}} + V_{\mathrm{d}}\dot{\gamma}_{\mathrm{d}}\right)\left(V_{\mathrm{d}}\ddot{\gamma}_{\mathrm{d}} - g\dot{\gamma}_{\mathrm{d}}\sin\gamma_{\mathrm{d}}\right) + V_{\mathrm{d}}^2\left(\dot{\chi}_{\mathrm{d}}\ddot{\chi}_{\mathrm{d}}\cos^2\gamma_{\mathrm{d}} - \dot{\chi}_{\mathrm{d}}^2\cos\gamma_{\mathrm{d}}\sin\gamma_{\mathrm{d}}\right)\right)}{(\bar{\rho}C_{L_{\mathrm{d}}})^2 - 2m^2 V_{\mathrm{d}}\left(\dot{\gamma}_{\mathrm{d}}\left(g\cos\gamma_{\mathrm{d}} + V_{\mathrm{d}}\dot{\gamma}_{\mathrm{d}}\right) + \dot{\chi}_{\mathrm{d}}^2\cos^2\gamma_{\mathrm{d}}\right)} \tag{20}$$

and compute the numerical solution online, as it is required by the control law.

In certain cases, it is more convenient to express the desired climb and course angles in terms of the desired airspeed and turn radius. We denote the climb and course radius as $r_\gamma(t)$ and $r_\chi(t)$, respectively, and denote the climb and course rates as $\dot{\gamma} = V_{\mathrm{d}}/r_\gamma$ and $\dot{\chi} = V_{\mathrm{d}}/r_\chi$. Using this structure, the desired bank angle and airspeed can be expressed as:

$$\mu_{\mathrm{d}} = \tan^{-1}\left(\frac{m\cos\gamma_{\mathrm{d}}/r_\chi}{\sqrt{(\bar{\rho}C_{L_{\mathrm{d}}} - m\cos\gamma_{\mathrm{d}}/r_\chi)(\bar{\rho}C_{L_{\mathrm{d}}} + m\cos\gamma_{\mathrm{d}}/r_\chi)}}\right) \tag{21}$$

$$V_{\mathrm{d}} = \sqrt{\frac{mg\cos\gamma_{\mathrm{d}}}{\sqrt{(\bar{\rho}C_{L_{\mathrm{d}}} - m\cos\gamma_{\mathrm{d}}/r_\chi)(\bar{\rho}C_{L_{\mathrm{d}}} + m\cos\gamma_{\mathrm{d}}/r_\chi)} - m/r_\gamma}} \tag{22}$$

While $\boldsymbol{\omega}_{\mathrm{d}}$ represents the desired angular velocity at steady state, using it as a reference signal may not satisfy conditions required for stability. Instead, we design state-dependent "target" quantities, denoted with the subscript "t", that converge to their respective desired values at steady state:

$$\boldsymbol{\omega}_{\mathrm{t}}(\alpha, \beta, \boldsymbol{\zeta}, \boldsymbol{\lambda}) = \boldsymbol{R}_{BW_{\mathrm{d}}}\bar{\boldsymbol{\omega}} - k\left(\frac{k_v}{2}\boldsymbol{R}_{BW}\left(\frac{\sin 2\tilde{\alpha}}{\cos\beta}\boldsymbol{e}_2 - \sin 2\beta\boldsymbol{e}_3\right) - k_\zeta\hat{\boldsymbol{\zeta}}_{\mathrm{d}}\boldsymbol{\zeta} - k_\lambda\hat{\boldsymbol{\lambda}}_{\mathrm{d}}\boldsymbol{\lambda}\right) \tag{23}$$

where $\tilde{\alpha} = \alpha - \alpha_{\mathrm{d}}$ and where $k > 0$ and k_v, k_ζ, $k_\lambda > 1$ are design parameters. Define the function

$$\mathscr{H}_{\mathrm{c}} = \frac{1}{2}(\boldsymbol{h} - \boldsymbol{I}\boldsymbol{\omega}_{\mathrm{t}})^{\mathrm{T}}\boldsymbol{I}^{-1}(\boldsymbol{h} - \boldsymbol{I}\boldsymbol{\omega}_{\mathrm{t}}) + \frac{m}{2}(V - V_{\mathrm{d}})^2 + \frac{k_v}{2}\left(\sin^2(\alpha - \alpha_{\mathrm{d}}) + \sin^2\beta\right) - k_\zeta\boldsymbol{\zeta}^{\mathrm{T}}\boldsymbol{\zeta}_{\mathrm{d}} - k_\lambda\boldsymbol{\lambda}^{\mathrm{T}}\boldsymbol{\lambda}_{\mathrm{d}} + \Phi_{\mathrm{c}} \tag{24}$$

where $\Phi_{\mathrm{c}} = \frac{1}{2}\left(k_\zeta(\boldsymbol{\zeta}^{\mathrm{T}}\boldsymbol{\zeta} + \boldsymbol{\zeta}_{\mathrm{d}}^{\mathrm{T}}\boldsymbol{\zeta}_{\mathrm{d}}) + k_\lambda(\boldsymbol{\lambda}^{\mathrm{T}}\boldsymbol{\lambda} + \boldsymbol{\lambda}_{\mathrm{d}}^{\mathrm{T}}\boldsymbol{\lambda}_{\mathrm{d}})\right)$ is a positive function of conserved quantities that is obtained using the energy-Casimir method. The control-modified Hamiltonian $\mathscr{H}_{\mathrm{c}}$ can be broken down as $\mathscr{H}_{\mathrm{c}} = \mathscr{H}_{\mathrm{t}} + \mathscr{H}_{\mathrm{v}} + \mathscr{H}_{\eta} + \Phi_{\mathrm{c}}$, where $\mathscr{H}_{\mathrm{t}} = \frac{1}{2}(\boldsymbol{h} - \boldsymbol{I}\boldsymbol{\omega}_{\mathrm{t}})^{\mathrm{T}}\boldsymbol{I}^{-1}(\boldsymbol{h} - \boldsymbol{I}\boldsymbol{\omega}_{\mathrm{t}}) + \frac{m}{2}(V - V_{\mathrm{d}})^2$ represents the error in the system's kinetic energy, $\mathscr{H}_{\mathrm{v}} = \frac{k_v}{2}\left(\sin^2(\alpha - \alpha_{\mathrm{d}}) + \sin^2\beta\right)$ represents the error in the aerodynamic angles and $\mathscr{H}_{\eta} = -\frac{k_\zeta}{2}\zeta^{\mathrm{T}}\zeta_{\mathrm{d}} - \frac{k_\lambda}{2}\lambda^{\mathrm{T}}\lambda_{\mathrm{d}}$ represents the restoring artificial potential energy for the attitude.

Theorem 1. The control law

$$\boldsymbol{\tau}_{\mathrm{c}} = -\left[\mathbb{I} \quad -\boldsymbol{I}\frac{\partial\boldsymbol{\omega}_{\mathrm{t}}}{\partial\boldsymbol{p}} \quad -\boldsymbol{I}\frac{\partial\boldsymbol{\omega}_{\mathrm{t}}}{\partial\boldsymbol{\eta}}\right](\boldsymbol{J} - \boldsymbol{D})\frac{\partial\tilde{\mathscr{H}}}{\partial\boldsymbol{x}}^{\mathrm{T}} - \boldsymbol{I}\frac{\partial\boldsymbol{\omega}_{\mathrm{t}}}{\partial\boldsymbol{x}}(\boldsymbol{J} - \boldsymbol{D})^{\mathrm{T}}\left[\boldsymbol{0} \quad \frac{\partial\mathscr{H}_{\mathrm{v}}}{\partial\boldsymbol{p}} \quad \frac{\partial(\mathscr{H}_{\eta} + \mathscr{H})}{\partial\boldsymbol{x}}\right]^{\mathrm{T}} - \frac{\partial\boldsymbol{\omega}_{\mathrm{t}}}{\partial t} - \mathscr{C}(\boldsymbol{\omega} - \boldsymbol{\omega}_{\mathrm{t}}), \tag{25}$$

$$F_{\mathrm{c}} = \frac{m\left[\boldsymbol{0}, -\boldsymbol{e}_1, \boldsymbol{0}\right](\boldsymbol{J} - \boldsymbol{D})\left[\boldsymbol{\omega}_{\mathrm{t}}^{\mathrm{T}}, V_{\mathrm{d}}\boldsymbol{e}_1^{\mathrm{T}}, -\frac{\partial\mathscr{H}_{\mathrm{v}}}{\partial\boldsymbol{v}}, -\frac{\partial(mg\boldsymbol{e}_3^{\mathrm{T}}\boldsymbol{q})}{\partial\boldsymbol{\eta}}\right]^{\mathrm{T}} - \dot{V}_{\mathrm{d}} + \frac{k_v(V - V_{\mathrm{d}})mg}{2VV_{\mathrm{d}}}\left(\boldsymbol{e}_2^{\mathrm{T}}\boldsymbol{\zeta}_{\mathrm{d}}\sin 2\beta + \frac{\boldsymbol{e}_3^{\mathrm{T}}\boldsymbol{R}_{BW_{\mathrm{d}}}^{\mathrm{T}}\boldsymbol{\zeta}_{\mathrm{d}}\sin 2\tilde{\alpha}}{\cos\beta}\right)}{\cos\tilde{\alpha}\cos\beta}, \tag{26}$$

where $\tilde{\mathcal{H}} = \mathcal{H} - \mathcal{H}_{\mathrm{c}}$ and $\mathscr{C} \succ 0$, asymptotically stabilizes the desired equilibrium.

Remark 1. Implementing the control law requires knowledge of the aerodynamic force and moment coefficients, but the proof does not require their explicit functional form. See comments following (12).

Proof of Theorem 1. Taking $\mathcal{H}_{\mathrm{c}}$ as a candidate Lyapunov function, we find

$$
\begin{aligned}
\dot{\mathcal{H}}_{\mathrm{c}} &= \frac{\partial \mathcal{H}_{\mathrm{c}}}{\partial \boldsymbol{x}} \left((\boldsymbol{J} - \boldsymbol{D}) \frac{\partial \mathcal{H}}{\partial \boldsymbol{x}}^{\mathrm{T}} + \boldsymbol{g} \boldsymbol{u} \right) + \frac{\partial \mathcal{H}_{\mathrm{c}}}{\partial t} \\
&= \frac{\partial \mathcal{H}_{\mathrm{c}}}{\partial \boldsymbol{x}} \left((\boldsymbol{J} - \boldsymbol{D}) \frac{\partial \tilde{\mathcal{H}}}{\partial \boldsymbol{x}}^{\mathrm{T}} + \boldsymbol{g} \boldsymbol{u} \right) - \frac{\partial \mathcal{H}_{\mathrm{c}}}{\partial \boldsymbol{x}} \boldsymbol{D} \frac{\partial \mathcal{H}_{\mathrm{c}}}{\partial \boldsymbol{x}}^{\mathrm{T}} + \frac{\partial \mathcal{H}_{\mathrm{c}}}{\partial t}
\end{aligned} \tag{27}
$$

With the proposed control moment, $\boldsymbol{\tau}_{\mathrm{c}}$, in equation (25) and the proposed control force, F_{c}, in equation (26), the time derivative of the proposed Hamiltonian function becomes:

$$
\begin{aligned}
\dot{\mathcal{H}}_{\mathrm{c}} = &-\frac{\partial \mathcal{H}_{\mathrm{c}}}{\partial \boldsymbol{x}} \boldsymbol{D} \frac{\partial \mathcal{H}_{\mathrm{c}}}{\partial \boldsymbol{x}}^{\mathrm{T}} - (\boldsymbol{\omega} - \boldsymbol{\omega}_{\mathrm{t}})^{\mathrm{T}} \mathscr{C} (\boldsymbol{\omega} - \boldsymbol{\omega}_{\mathrm{t}}) + \frac{\partial (\mathcal{H}_{\mathrm{c}} - \mathcal{H}_{\mathrm{t}})}{\partial t} \\
&+ \frac{k_v (V - V_{\mathrm{d}}) g}{2 V V_{\mathrm{d}}} \left(\zeta_{2_{\mathrm{d}}} \sin 2\beta + \frac{\boldsymbol{e}_3^{\mathrm{T}} \boldsymbol{R}_{BW_{\mathrm{d}}}^{\mathrm{T}} \boldsymbol{\zeta}_{\mathrm{d}} \sin 2\tilde{\alpha}}{\cos \beta} \right) \\
&+ \left[\boldsymbol{0}_{1 \times 3} \quad \frac{\partial \mathcal{H}_v}{\partial \boldsymbol{v}} \quad \frac{\partial \mathcal{V}_{\mathrm{d}}}{\partial \boldsymbol{\eta}} \right] (\boldsymbol{J} - \boldsymbol{D}) \left[\boldsymbol{\omega}_{\mathrm{t}}^{\mathrm{T}} \quad V_{\mathrm{d}} \boldsymbol{e}_1^{\mathrm{T}} \quad \frac{\partial \mathcal{H}_v}{\partial \boldsymbol{v}} \quad \frac{\partial \mathcal{V}}{\partial \boldsymbol{\eta}} - \frac{\partial \mathcal{V}_{\mathrm{d}}}{\partial \boldsymbol{\eta}} \right]^{\mathrm{T}}
\end{aligned} \tag{28}
$$

Taking advantage of the structure and sparsity of $\boldsymbol{J}$ reduces equation (28) to

$$
\begin{aligned}
\dot{\mathcal{H}}_{\mathrm{c}} = &-\frac{\partial \mathcal{H}_{\mathrm{t}}}{\partial \boldsymbol{x}} \boldsymbol{D} \frac{\partial \mathcal{H}_{\mathrm{t}}}{\partial \boldsymbol{x}}^{\mathrm{T}} - (\boldsymbol{\omega} - \boldsymbol{\omega}_{\mathrm{t}})^{\mathrm{T}} \mathscr{C} (\boldsymbol{\omega} - \boldsymbol{\omega}_{\mathrm{t}}) + \frac{\partial (\mathcal{H}_{\mathrm{c}} - \mathcal{H}_{\mathrm{t}})}{\partial t} \\
&+ \frac{k_v (V - V_{\mathrm{d}}) g}{2 V V_{\mathrm{d}}} \left(\boldsymbol{e}_2^{\mathrm{T}} \boldsymbol{\zeta} \sin 2\beta + \frac{\boldsymbol{e}_3^{\mathrm{T}} \boldsymbol{R}_{BW}^{\mathrm{T}} \boldsymbol{\zeta} \sin 2\tilde{\alpha}}{\cos \beta} \right) \\
&+ \left[\boldsymbol{0}_{1 \times 3} \quad \frac{\partial \mathcal{H}_v}{\partial \boldsymbol{v}} \quad \frac{\partial \mathcal{V}_{\mathrm{d}}}{\partial \boldsymbol{\eta}} \right] (\boldsymbol{J} - \boldsymbol{D}) \left[\boldsymbol{\omega}_{\mathrm{t}}^{\mathrm{T}} \quad V_{\mathrm{d}} \boldsymbol{e}_1^{\mathrm{T}} \quad \frac{\partial \mathcal{V}}{\partial \boldsymbol{\eta}} \right]^{\mathrm{T}}
\end{aligned} \tag{29}
$$

Expanding (29) and substituting for the control thrust F_{c} from equation (26) gives:

$$
\begin{aligned}
\dot{\mathcal{H}}_{\mathrm{c}} = &-(\boldsymbol{\omega} - \boldsymbol{\omega}_{\mathrm{t}})^{\mathrm{T}} (\mathscr{C} + \boldsymbol{D}_\omega) (\boldsymbol{\omega} - \boldsymbol{\omega}_{\mathrm{t}}) - \bar{\rho} V C_D (V - V_{\mathrm{d}})^2 \\
&+ k_v \frac{\sin \beta \cos \beta}{m} \left(-m \boldsymbol{e}_3^{\mathrm{T}} \boldsymbol{R}_{BW} \boldsymbol{\omega}_{\mathrm{t}} - \bar{\rho} V_{\mathrm{d}} C_S + \frac{mg \boldsymbol{e}_2^{\mathrm{T}} \boldsymbol{R}_{BW}^{\mathrm{T}} \boldsymbol{\zeta}}{V} - \frac{\tan \beta}{V} \bar{F}_{\mathrm{c}} \right) \\
&+ k_v \frac{\sin \tilde{\alpha} \cos \tilde{\alpha}}{m \cos \beta} \left(m \boldsymbol{e}_2^{\mathrm{T}} \boldsymbol{R}_{BW} \boldsymbol{\omega}_{\mathrm{t}} - \bar{\rho} V_{\mathrm{d}} C_L + \frac{mg \boldsymbol{e}_3^{\mathrm{T}} \boldsymbol{R}_{BW}^{\mathrm{T}} \boldsymbol{\zeta}}{V} - \frac{\tan \tilde{\alpha}}{V \cos \beta} \bar{F}_{\mathrm{c}} \right) \\
&- k_\zeta \left(\boldsymbol{\zeta}_{\mathrm{d}}^{\mathrm{T}} \hat{\boldsymbol{\zeta}} \boldsymbol{\omega}_{\mathrm{t}} + \boldsymbol{\zeta}^{\mathrm{T}} \dot{\boldsymbol{\zeta}}_{\mathrm{d}} \right) - k_\lambda \left(\boldsymbol{\lambda}_{\mathrm{d}}^{\mathrm{T}} \hat{\boldsymbol{\lambda}} \boldsymbol{\omega}_{\mathrm{t}} + \boldsymbol{\lambda}^{\mathrm{T}} \dot{\boldsymbol{\lambda}}_{\mathrm{d}} \right) \\
&+ \frac{k_v (V - V_{\mathrm{d}}) g}{2 V V_{\mathrm{d}}} \left(\zeta_2 \sin 2\beta + \frac{\boldsymbol{e}_3^{\mathrm{T}} \boldsymbol{R}_{BW}^{\mathrm{T}} \boldsymbol{\zeta} \sin 2\tilde{\alpha}}{\cos \beta} \right)
\end{aligned} \tag{30}
$$

where $\bar{F}_{\mathrm{c}} = F_{\mathrm{c}} \cos \tilde{\alpha} \cos \beta$ would be the proposed control law were the thrust pointing along the velocity vector. The time rate of the desired attitude vectors can be expressed in terms of $\bar{\boldsymbol{\omega}}$ as

$$
\dot{\boldsymbol{\zeta}}_{\mathrm{d}} = \hat{\boldsymbol{\zeta}}_{\mathrm{d}} \boldsymbol{R}_{BW_{\mathrm{d}}} \bar{\boldsymbol{\omega}}, \; \dot{\boldsymbol{\lambda}}_{\mathrm{d}} = \hat{\boldsymbol{\lambda}}_{\mathrm{d}} \boldsymbol{R}_{BW_{\mathrm{d}}} \bar{\boldsymbol{\omega}} \tag{31}
$$

Inserting the equations from (31) in (30) and reducing the equation further gives

$$
\begin{aligned}
\dot{\mathscr{H}}_\text{c} ={}& -(\boldsymbol{\omega}-\boldsymbol{\omega}_\text{t})^\text{T}(\mathscr{C}+\boldsymbol{D}_\omega)(\boldsymbol{\omega}-\boldsymbol{\omega}_\text{t}) - \bar{\rho}VC_D(V-V_\text{d})^2 \\
&+ k_v\frac{\sin\beta\cos\beta}{m}\left(-m\boldsymbol{e}_3^\text{T}\boldsymbol{R}_{BW}\boldsymbol{\omega}_\text{t} - \bar{\rho}V_\text{d}C_S + mg\left(\frac{\boldsymbol{e}_2^\text{T}\boldsymbol{R}_{BW}^\text{T}\boldsymbol{\zeta}}{V} + \frac{(V-V_\text{d})\zeta_{2_\text{d}}}{VV_\text{d}}\right) - \frac{\tan\beta}{V}\bar{F}_\text{c}\right) \\
&+ k_v\frac{\sin\tilde{\alpha}\cos\tilde{\alpha}}{m\cos\beta}\left(m\boldsymbol{e}_2^\text{T}\boldsymbol{R}_{BW}\boldsymbol{\omega}_\text{t} - \bar{\rho}V_\text{d}C_L + mg\boldsymbol{e}_3^\text{T}\left(\frac{\boldsymbol{R}_{BW}^\text{T}\boldsymbol{\zeta}}{V} + \frac{(V-V_\text{d})\boldsymbol{R}_{BW_\text{d}}^\text{T}\boldsymbol{\zeta}_\text{d}}{VV_\text{d}}\right) - \frac{\tan\tilde{\alpha}}{V\cos\beta}\bar{F}_\text{c}\right) \\
&+ \left(k_\zeta\boldsymbol{\zeta}^\text{T}\hat{\boldsymbol{\zeta}}_\text{d} + k_\lambda\boldsymbol{\lambda}^\text{T}\hat{\boldsymbol{\lambda}}_\text{d}\right)(\boldsymbol{\omega}_\text{t} - \boldsymbol{R}_{BW_\text{d}}\bar{\boldsymbol{\omega}})
\end{aligned}
\tag{32}
$$

Next, we substitute $\boldsymbol{\omega}_\text{t}$ from (23) above, observe that $\boldsymbol{R}_{BW} = \boldsymbol{R}_{BW_\text{d}} + (\mathbb{I}-\boldsymbol{R}_{BW_\text{d}}\boldsymbol{R}_{BW}^\text{T})\boldsymbol{R}_{BW}$, and substitute $\bar{\omega}_2$ and $\bar{\omega}_3$ from (23) and μ_d from (18) to obtain:

$$
\begin{aligned}
\dot{\mathscr{H}}_\text{c} ={}& -(\boldsymbol{\omega}-\boldsymbol{\omega}_\text{t})^\text{T}(\mathscr{C}+\boldsymbol{D}_\omega)(\boldsymbol{\omega}-\boldsymbol{\omega}_\text{t}) - \bar{\rho}VC_D(V-V_\text{d})^2 \\
&+ k_v\frac{\sin\beta\cos\beta}{m}\bigg(m\boldsymbol{e}_3^\text{T}\left(\mathbb{I}-\boldsymbol{R}_{BW}^\text{T}\boldsymbol{R}_{BW_\text{d}}\right)\bar{\boldsymbol{\omega}} - \bar{\rho}V_\text{d}C_S \\
&\qquad\qquad +mg\boldsymbol{e}_2^\text{T}\left(\frac{(\mathbb{I}-\boldsymbol{R}_{BW_\text{d}}^\text{T}\boldsymbol{R}_{BW})\boldsymbol{R}_{BW}^\text{T}\boldsymbol{\zeta}_\text{d} + \boldsymbol{R}_{BW}^\text{T}(\boldsymbol{\zeta}-\boldsymbol{\zeta}_\text{d})}{V}\right) - \frac{\tan\beta}{V}\bar{F}_\text{c}\bigg) \\
&+ k_v\frac{\sin\tilde{\alpha}\cos\tilde{\alpha}}{m\cos\beta}\bigg(-m\boldsymbol{e}_2^\text{T}\left(\mathbb{I}-\boldsymbol{R}_{BW}^\text{T}\boldsymbol{R}_{BW_\text{d}}\right)\bar{\boldsymbol{\omega}} - \bar{\rho}V_\text{d}(C_L-C_{L_\text{d}}) \\
&\qquad\qquad +mg\boldsymbol{e}_3^\text{T}\left(\frac{(\mathbb{I}-\boldsymbol{R}_{BW_\text{d}}^\text{T}\boldsymbol{R}_{BW})\boldsymbol{R}_{BW}^\text{T}\boldsymbol{\zeta}_\text{d} + \boldsymbol{R}_{BW}^\text{T}(\boldsymbol{\zeta}-\boldsymbol{\zeta}_\text{d})}{V}\right) - \frac{\tan\tilde{\alpha}}{V\cos\beta}\bar{F}_\text{c}\bigg) \\
&- k\left\|\frac{k_v}{2}\boldsymbol{R}_{BW}\left(\frac{\sin 2\tilde{\alpha}}{\cos\beta}\boldsymbol{e}_2 - \sin 2\beta\boldsymbol{e}_3\right) - k_\zeta\hat{\boldsymbol{\zeta}}_\text{d}\boldsymbol{\zeta} - k_\lambda\hat{\boldsymbol{\lambda}}_\text{d}\boldsymbol{\lambda}\right\|^2
\end{aligned}
\tag{33}
$$

One can verify that $\left\|\boldsymbol{e}_2^\text{T}(\mathbb{I}-\boldsymbol{R}_{BW}^\text{T}\boldsymbol{R}_{BW_\text{d}})\right\| \le \sqrt{2}|\sin\beta|$ and that $\left\|\boldsymbol{e}_3^\text{T}(\mathbb{I}-\boldsymbol{R}_{BW}^\text{T}\boldsymbol{R}_{BW_\text{d}})\right\| \le \sqrt{2}|\sin\tilde{\alpha}|$. The terms which include $(\mathbb{I}-\boldsymbol{R}_{BW}^\text{T}\boldsymbol{R}_{BW_\text{d}})$ result from deviations in the aerodynamic angles when all other variables are at their steady state values. For a stable aircraft and a well-posed $\bar{\boldsymbol{\omega}}$, these terms are dominated by the restoring effect of the lift and side force. Based on the assumptions on the aerodynamic coefficients, one may conclude that both $C_S\sin\beta$ and $(C_L-C_{L_\text{d}})\sin\tilde{\alpha}$ are non-negative. Furthermore, assuming that $C_S\sin\beta \ge k_s\sin^2\beta$ and $(C_L-C_{L_\text{d}})\sin\tilde{\alpha} \ge k_L\sin^2\tilde{\alpha}$, one may show that

$$
\begin{aligned}
\dot{\mathscr{H}}_\text{c} \le{}& -(\boldsymbol{\omega}-\boldsymbol{\omega}_\text{t})^\text{T}(\mathscr{C}+\boldsymbol{D}_\omega)(\boldsymbol{\omega}-\boldsymbol{\omega}_\text{t}) - \bar{\rho}VC_D(V-V_\text{d})^2 \\
&- [|\sin\beta|,\ |\sin\tilde{\alpha}|]\boldsymbol{K}_v[|\sin\beta|,\ |\sin\tilde{\alpha}|]^\text{T} + \frac{k_vg}{V}\left(|\sin\beta|\cos\beta + \frac{|\sin\tilde{\alpha}|\cos\tilde{\alpha}}{\cos\beta}\right)\|\boldsymbol{\zeta}-\boldsymbol{\zeta}_\text{d}\| \\
&- k\left\|\frac{k_v}{2}\boldsymbol{R}_{BW}\left(\frac{\sin 2\tilde{\alpha}}{\cos\beta}\boldsymbol{e}_2 - \sin 2\beta\boldsymbol{e}_3\right) - k_\zeta\hat{\boldsymbol{\zeta}}_\text{d}\boldsymbol{\zeta} - k_\lambda\hat{\boldsymbol{\lambda}}_\text{d}\boldsymbol{\lambda}\right\|^2
\end{aligned}
\tag{34}
$$

where

$$
\boldsymbol{K}_v = \frac{k_v}{m}\begin{bmatrix} \cos\beta\left(\bar{\rho}V_\text{d}K_S + \frac{\bar{F}_\text{c}}{V\cos\beta} - \frac{\sqrt{2}mg}{V}\right) & -\frac{m\|\bar{\boldsymbol{\omega}}\|}{\sqrt{2}}\left(\cos\beta + \frac{\cos\tilde{\alpha}}{\cos\beta}\right) \\ -\frac{m\|\bar{\boldsymbol{\omega}}\|}{\sqrt{2}}\left(\cos\beta + \frac{\cos\tilde{\alpha}}{\cos\beta}\right) & \frac{\cos\tilde{\alpha}}{\cos\beta}\left(\bar{\rho}V_\text{d}K_L + \frac{\bar{F}_\text{c}}{V\cos\tilde{\alpha}\cos\beta} - \frac{\sqrt{2}mg}{V}\right) \end{bmatrix}
\tag{35}
$$

Note that the first term of (34) is non-positive since $\boldsymbol{D}_\omega \succeq 0$ and $\mathscr{C} \succ 0$, in addition to the fact that C_D is positive so that $-\bar{\rho}C_DV(V-V_\text{t})^2 \le 0$. For reasons stated earlier, $\boldsymbol{K}_v \succ 0$. Therefore, the first term in the second line of inequality (34) is non-positive. Similarly, the last term of the inequality is non-positive

as well. To ensure that $\dot{\mathscr{H}}_c$ is non-positive, one must choose

$$k \geq \sqrt{\frac{2k_v g}{k_\zeta \|\boldsymbol{K}_v\| \min(V)} \max\left(\cos\beta, \frac{\cos\tilde{\alpha}}{\cos\beta}\right)} \tag{36}$$

The conditions for Lyapunov stability must hold within level sets of $\mathscr{H}_c$. Because the value of the Lyapunov function is minimum at the desired state of motion, by choosing a sufficiently small level set, one can ensure that the minimum airspeed (i.e., $\min V$) is sufficiently large that one may choose a feasible value of k and therefore that $\dot{\mathscr{H}}_c \leq 0$, showing that the desired equilibrium is stable. $\square$

5 Cross-Track Control

Having established a control law which asymptotically stabilizes the motion of a fixed wing aircraft to a smoothly time-varying, non-vertical inertial direction, it is possible to achieve cross-track control by varying the direction of motion with respect to position instead of time. In this work, only piecewise linear paths are considered, e.g., the linear segments connecting a sequence of three-dimensional waypoints. We use line-of-sight guidance as used, for example, by Encarnação and Pascoal [26], Børhaug and Pettersen [27], and Techy and Woolsey [25].

To simplify the presentation, suppose the desired linear path segment passes through the origin of the inertial frame and let $\boldsymbol{R}_d = e^{\chi_d \hat{\boldsymbol{e}}_3} e^{\gamma_d \hat{\boldsymbol{e}}_2}$, where the desired climb and course angles define the desired velocity direction, with a desired bank angle of zero. Let $\boldsymbol{d}$ be a vector from the center of mass of the aircraft to a "look-ahead" point along the desired linear path segment:

$$\boldsymbol{d} = L_k \boldsymbol{e}_1 - (\mathbb{I} - \boldsymbol{e}_1 \boldsymbol{e}_1^T) \boldsymbol{R}_d^T \boldsymbol{q} \tag{37}$$

The parameter L_k is a prescribed look-ahead distance from the point on the line nearest the aircraft to the look-ahead point. The vector $\boldsymbol{d}$ is the vector difference of this look-ahead vector and the cross-track error vector; it defines the direction the aircraft should fly to converge smoothly to the path segment.

Now define a target rotation matrix $\boldsymbol{R}_t = e^{\chi_t \hat{\boldsymbol{e}}_3} e^{\gamma_t \hat{\boldsymbol{e}}_2} e^{\mu_t \hat{\boldsymbol{e}}_1}$ based on the cross-track guidance law, where

$$\gamma_t = -\sin^{-1}\left(\frac{\boldsymbol{e}_3^T \boldsymbol{d}}{\|\boldsymbol{d}\|}\right) \tag{38}$$

$$\chi_t = \sin^{-1}\left(\frac{\boldsymbol{e}_2^T \boldsymbol{d}}{\|\boldsymbol{d}\|}\right) \tag{39}$$

$$\mu_t = \tan^{-1}\left(\frac{m\boldsymbol{e}_2^T \bar{\boldsymbol{d}} \cos\gamma_t / \cos\chi_t}{\sqrt{(\bar{\rho}C_{L_d} - m\boldsymbol{e}_2^T \bar{\boldsymbol{d}} \cos\gamma_t / \cos\chi_t)(\bar{\rho}C_{L_d} + m\boldsymbol{e}_2^T \bar{\boldsymbol{d}} \cos\gamma_t / \cos\chi_t)}}\right) \tag{40}$$

$$V_d = \sqrt{\frac{mg\cos\gamma_t}{\sqrt{(\bar{\rho}C_{L_d} - m\boldsymbol{e}_2^T \bar{\boldsymbol{d}} \cos\gamma_t / \cos\chi_t)(\bar{\rho}C_{L_d} + m\boldsymbol{e}_2^T \bar{\boldsymbol{d}} \cos\gamma_t / \cos\chi_t)} - m\boldsymbol{e}_3^T \bar{\boldsymbol{d}} / \cos\gamma_t}} \tag{41}$$

and where

$$\bar{\boldsymbol{d}} = \frac{1}{\|\boldsymbol{d}\|}\left(\mathbb{I} - \frac{\boldsymbol{d}\boldsymbol{d}^T}{\boldsymbol{d}^T \boldsymbol{d}}\right)\left(\mathbb{I} - \boldsymbol{e}_1 \boldsymbol{e}_1^T\right) \boldsymbol{R}_t \boldsymbol{e}_1 \tag{42}$$

10

Let the desired attitude vectors in (6) be $\boldsymbol{\zeta}_\text{d} = \boldsymbol{R}_{IB_\text{d}}^\text{T} \boldsymbol{e}_3$ and $\boldsymbol{\lambda}_\text{d} = \boldsymbol{R}_{IB_\text{d}}^\text{T} \boldsymbol{e}_1$, where $\boldsymbol{R}_{IB_\text{d}} = \boldsymbol{R}_\text{d} \boldsymbol{R}_\text{t} \boldsymbol{R}_{BW_\text{d}}^\text{T}$. The desired angular velocity, expressed in the wind frame, is

$$\bar{\boldsymbol{\omega}} = \mathring{\mu}_\text{t} \boldsymbol{e}_1 + e^{-\mu_\text{t} \hat{\boldsymbol{e}}_1} \left(\mathring{\gamma}_\text{t} \boldsymbol{e}_2 + \mathring{\chi}_\text{t} e^{-\gamma_\text{t} \hat{\boldsymbol{e}}_2} \boldsymbol{e}_3 \right) \tag{43}$$

where, for an arbitrary, smooth function $\delta(\boldsymbol{q})$ of the aircraft position,

$$\mathring{\delta}(\boldsymbol{q}) = \frac{\partial \delta(\boldsymbol{q})}{\partial \boldsymbol{q}} \boldsymbol{R}_{IB_\text{d}} \boldsymbol{R}_{BW_\text{d}} \boldsymbol{e}_1 V_\text{d} = \frac{\partial \delta(\boldsymbol{q})}{\partial \boldsymbol{q}} \boldsymbol{R}_\text{d} \boldsymbol{R}_\text{t} \boldsymbol{e}_1 V_\text{d} \tag{44}$$

Remark 2. Using $(\mathring{\cdot})$ rather than the true time derivative ensures that the desired angular velocity $\bar{\boldsymbol{\omega}}$ obtained from the cross-track guidance geometry does not depend on the true angular velocity $\boldsymbol{\omega}$. Recognizing a separation of time scales – i.e., that the aircraft attitude converges instantly to a commanded orientation, relative to the time scale of cross-track convergence – we have defined the desired angular velocity $\bar{\boldsymbol{\omega}}$ solely in terms of the cross-track error.

The original definition in equation (23) is used for the target angular rate $\boldsymbol{\omega}_\text{t}$, but using equation (43) for $\bar{\boldsymbol{\omega}}$. To prove stability of the cross-track control system, the following candidate Lyapunov function is proposed: $\mathscr{H}_\text{c} = \mathscr{H}_\text{t} + \mathscr{H}_\text{v} + \mathscr{H}_\eta + \Phi_\text{c}$, where

$$\mathscr{H}_\text{t} = \frac{1}{2} (\boldsymbol{h} - \boldsymbol{I} \boldsymbol{\omega}_\text{t})^\text{T} \boldsymbol{I}^{-1} (\boldsymbol{h} - \boldsymbol{I} \boldsymbol{\omega}_\text{t}) + \frac{m}{2} (V - V_\text{d})^2 \tag{45}$$

$$\mathscr{H}_\text{v} = \frac{k_v}{2} \left(\sin^2(\alpha - \alpha_\text{d}) + \sin^2 \beta \right) \tag{46}$$

$$\mathscr{H}_\eta = -\frac{k_\zeta}{2} \boldsymbol{\zeta}^\text{T} \boldsymbol{\zeta}_\text{d} - \frac{k_\lambda}{2} \boldsymbol{\lambda}^\text{T} \boldsymbol{\lambda}_\text{d} - k_q \boldsymbol{e}_1^\text{T} \boldsymbol{d} / \|\boldsymbol{d}\| \tag{47}$$

$$\Phi_\text{c} = \frac{1}{2} \left(k_\zeta (\boldsymbol{\zeta}^\text{T} \boldsymbol{\zeta} + \boldsymbol{\zeta}_\text{d}^\text{T} \boldsymbol{\zeta}_\text{d}) + k_\lambda (\boldsymbol{\lambda}^\text{T} \boldsymbol{\lambda} + \boldsymbol{\lambda}_\text{d}^\text{T} \boldsymbol{\lambda}_\text{d}) + 2 k_q \right) \tag{48}$$

Note that the proposed Lyapunov function for cross-track control is the same as that for time-varying directional stabilization except for the addition of the expression $k_q (\boldsymbol{d} / \|\boldsymbol{d}\| - \boldsymbol{e}_1)^\text{T} (\boldsymbol{d} / \|\boldsymbol{d}\| - \boldsymbol{e}_1) / 2$.

Theorem 2. The control law structure given in equations (25) and (26), but using equations (38-48), asymptotically stabilizes the desired steady motion.

Proof. The proof follows similarly to that in Section 4 up until equation (32). The time derivative of the Lyapunov function becomes:

$$\begin{aligned} \dot{\mathscr{H}}_\text{c} = &-(\boldsymbol{\omega} - \boldsymbol{\omega}_\text{t})^\text{T} (\mathscr{C} + \boldsymbol{D}_\omega)(\boldsymbol{\omega} - \boldsymbol{\omega}_\text{t}) - \bar{\rho} V C_D (V - V_\text{d})^2 \\ &+ k_v \frac{\sin \beta \cos \beta}{m} \left(-m \boldsymbol{e}_3^\text{T} \boldsymbol{R}_{BW} \boldsymbol{\omega}_\text{t} - \bar{\rho} V_\text{d} C_S + mg \left(\frac{\boldsymbol{e}_2^\text{T} \boldsymbol{R}_{BW}^\text{T} \boldsymbol{\zeta}}{V} + \frac{(V - V_\text{d}) \zeta_{2_\text{d}}}{V V_\text{d}} \right) - \frac{\tan \beta}{V} \bar{F}_\text{c} \right) \\ &+ k_v \frac{\sin \tilde{\alpha} \cos \tilde{\alpha}}{m \cos \beta} \left(m \boldsymbol{e}_2^\text{T} \boldsymbol{R}_{BW} \boldsymbol{\omega}_\text{t} - \bar{\rho} V_\text{d} C_L + mg \boldsymbol{e}_3^\text{T} \left(\frac{\boldsymbol{R}_{BW}^\text{T} \boldsymbol{\zeta}}{V} + \frac{(V - V_\text{d}) \boldsymbol{R}_{BW_\text{d}}^\text{T} \boldsymbol{\zeta}_\text{d}}{V V_\text{d}} \right) - \frac{\tan \tilde{\alpha}}{V \cos \beta} \bar{F}_\text{c} \right) \\ &+ \left(k_\zeta \boldsymbol{\zeta}^\text{T} \hat{\boldsymbol{\zeta}}_\text{d} + k_\lambda \boldsymbol{\lambda}^\text{T} \hat{\boldsymbol{\lambda}}_\text{d} \right) \boldsymbol{\omega}_\text{t} - V_\text{d} \left(k_\zeta \boldsymbol{\zeta}^\text{T} \frac{\partial \boldsymbol{\zeta}_\text{d}}{\partial \boldsymbol{d}} + k_\zeta \boldsymbol{\lambda}^\text{T} \frac{\partial \boldsymbol{\lambda}_\text{d}}{\partial \boldsymbol{d}} \right) \left(\mathbb{I} - \frac{\boldsymbol{d} \boldsymbol{d}^\text{T}}{\boldsymbol{d}^\text{T} \boldsymbol{d}} \right) (\mathbb{I} - \boldsymbol{e}_1 \boldsymbol{e}_1^\text{T}) \boldsymbol{R}_{IB} \boldsymbol{R}_{BW} \boldsymbol{e}_1 \\ &+ \frac{k_q V_\text{d}}{\sqrt{\boldsymbol{d}^\text{T} \boldsymbol{d}}} \boldsymbol{e}_1^\text{T} \left(\mathbb{I} - \frac{\boldsymbol{d} \boldsymbol{d}^\text{T}}{\boldsymbol{d}^\text{T} \boldsymbol{d}} \right) (\mathbb{I} - \boldsymbol{e}_1 \boldsymbol{e}_1^\text{T}) \boldsymbol{R}_{IB} \boldsymbol{R}_{BW} \boldsymbol{e}_1 \end{aligned} \tag{49}$$

Based on the definitions of $\bar{\boldsymbol{\omega}}$, $\boldsymbol{\zeta}_{\mathrm{d}}$ and $\boldsymbol{\lambda}_{\mathrm{d}}$, the following equalities hold:

$$\hat{\boldsymbol{\zeta}}_{\mathrm{d}}\bar{\boldsymbol{\omega}} = V_{\mathrm{d}}\frac{\partial \boldsymbol{\zeta}_{\mathrm{d}}}{\partial \boldsymbol{d}}\left(\mathbb{I}-\frac{\boldsymbol{d}\boldsymbol{d}^{\mathrm{T}}}{\boldsymbol{d}^{\mathrm{T}}\boldsymbol{d}}\right)\left(\mathbb{I}-\boldsymbol{e}_1\boldsymbol{e}_1^{\mathrm{T}}\right)\boldsymbol{R}_{IB_{\mathrm{d}}}\boldsymbol{R}_{BW_{\mathrm{d}}}\boldsymbol{e}_1 \tag{50}$$

$$\hat{\boldsymbol{\lambda}}_{\mathrm{d}}\bar{\boldsymbol{\omega}} = V_{\mathrm{d}}\frac{\partial \boldsymbol{\lambda}_{\mathrm{d}}}{\partial \boldsymbol{d}}\left(\mathbb{I}-\frac{\boldsymbol{d}\boldsymbol{d}^{\mathrm{T}}}{\boldsymbol{d}^{\mathrm{T}}\boldsymbol{d}}\right)\left(\mathbb{I}-\boldsymbol{e}_1\boldsymbol{e}_1^{\mathrm{T}}\right)\boldsymbol{R}_{IB_{\mathrm{d}}}\boldsymbol{R}_{BW_{\mathrm{d}}}\boldsymbol{e}_1 \tag{51}$$

Applying further reduction similar to those done in (33) and (34) gives:

$$\begin{aligned}
\dot{\mathscr{H}}_{\mathrm{c}} \leq & -(\boldsymbol{\omega}-\boldsymbol{\omega}_{\mathrm{t}})^{\mathrm{T}}(\mathscr{C}+\boldsymbol{D}_{\omega})(\boldsymbol{\omega}-\boldsymbol{\omega}_{\mathrm{t}})-\bar{\rho}VC_D(V-V_{\mathrm{d}})^2 \\
& -[|\sin\beta|, |\sin\tilde{\alpha}|]\boldsymbol{K}_v[|\sin\beta|, |\sin\tilde{\alpha}|]^{\mathrm{T}}+\frac{k_vg}{V}\left(|\sin\beta|\cos\beta+\frac{|\sin\tilde{\alpha}|\cos\tilde{\alpha}}{\cos\beta}\right)\|\boldsymbol{\zeta}-\boldsymbol{\zeta}_{\mathrm{d}}\| \\
& -k\left\|\frac{k_v}{2}\boldsymbol{R}_{BW}\left(\frac{\sin 2\tilde{\alpha}}{\cos\beta}\boldsymbol{e}_2-\sin 2\beta\boldsymbol{e}_3\right)-k_\zeta\hat{\boldsymbol{\zeta}}_{\mathrm{d}}\boldsymbol{\zeta}-k_\lambda\hat{\boldsymbol{\lambda}}_{\mathrm{d}}\boldsymbol{\lambda}\right\|^2 \\
& -\frac{L_k}{(\boldsymbol{d}^{\mathrm{T}}\boldsymbol{d})^2}\left((\boldsymbol{e}_3^{\mathrm{T}}\boldsymbol{d})^2+(\boldsymbol{e}_2^{\mathrm{T}}\boldsymbol{d})^2\cos\gamma_{\mathrm{t}}\right)+\frac{L_k\sqrt{2}}{\|\boldsymbol{d}\|^2}\left(\|\hat{\boldsymbol{\zeta}}\boldsymbol{\zeta}_{\mathrm{d}}\|+\|\hat{\boldsymbol{\lambda}}\boldsymbol{\lambda}_{\mathrm{d}}\|+|\sin\tilde{\alpha}|+|\sin\tilde{\beta}|\right)
\end{aligned} \tag{52}$$

where $\boldsymbol{K}_v$ is defined in equation (35). The first three lines of (52) are the same as in (34), which has been shown to be negative. The first term of the last line is a non-positive quadratic term in the cross-track error while the other terms are first order couplings between the cross-track error vector and the attitude error terms, as well as the error in the aerodynamic angles. The Lyapunov rate (52) has non-positive quadratic components in all those terms which are sufficiently large to ensure that $\dot{\mathscr{H}}_{\mathrm{c}} < 0$, showing that the desired equilibrium is asymptotically stable. $\square$

6 Simulation

To demonstrate the cross-track control law, we simulate its performance using a flight dynamic model obtained from flight tests of the My Twin Dream aircraft, as described in [28].
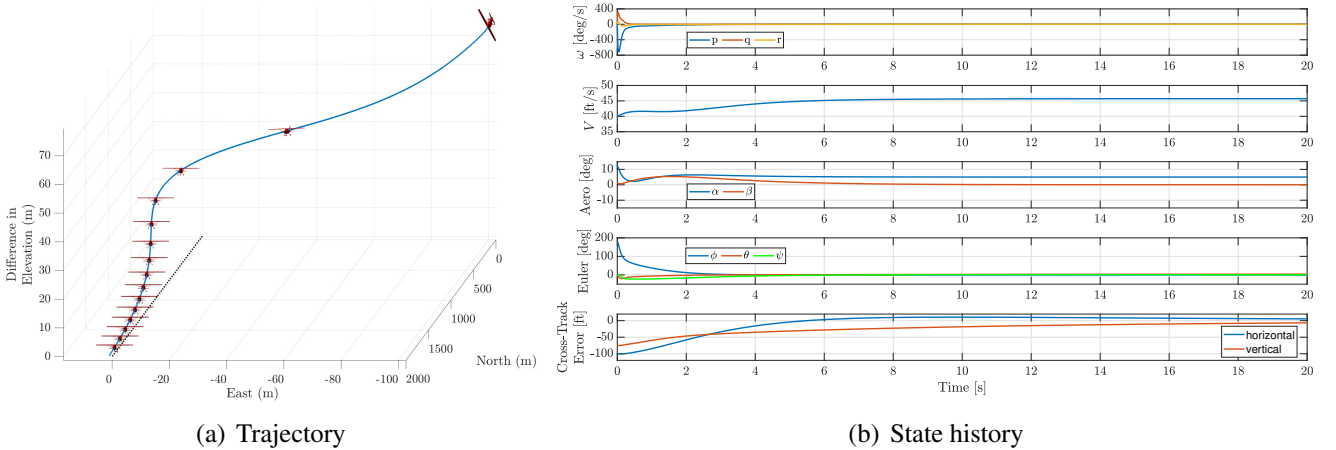

(a) Trajectory

(b) State history

Fig. 1 Left: Desired path (dotted black) and actual path (solid blue), with aircraft position and attitude denoted at two second intervals. Right: State history for the trajectory shown at the left.

In the simulation, the aircraft starts in inverted flight 100 ft west of and 75 ft above an inertial reference with an airspeed of 40 ft/s and with $\alpha = 10°$ and $\beta = 5°$. The desired path is along the positive $\boldsymbol{e}_1$ axis of the inertial frame (e.g., "due North"). Initial values for state variables other than velocity were chosen randomly. The results shown in Figure 1 reflect the analytical stability results presented earlier, although the simulation model incorporates aerodynamic interactions which were ignored in the control design and analysis, such as aerodynamic force terms involving angular rates.

Figure 1(a) shows the vehicle trajectory (solid line) using the proposed controller subject to the previously stated initial conditions. The aircraft's orientation is indicated at equal time steps by a 3D aircraft model (although the geometry is not that of the MTD). The feedback controlled trajectory converges to the desired flight profile. Figures 1(b) show the time history of rates and attitude variables.

7 Conclusion

A nonlinear, energy-based control design was presented for a small, fixed-wing aircraft which stabilizes the aircraft's flight to a non-vertical, piecewise linear path characterized by a course and climb angle. The cross-track control law is built upon directional stabilization results for a time-varying course and climb angle. The control law requires knowledge of some aerodynamic parameters, but the stability analysis uses very general assumptions about the aerodynamic forces and moments.

The nonlinear, energy-shaping control law, and the Lyapunov-based proof of nonlinear stability, leverages the passivity properties enjoyed by the port-Hamiltonian system model.

Ongoing work involves demonstrating the control law presented here in flight tests. Follow-on work will focus on extending the results to curvilinear path-following.

References

[1] S. A. Snell, D. F. Enns, and Jr. W. L. Garrard. Nonlinear inversion flight control for a supermaneuverable aircraft. *AIAA Journal of Guidance, Control, and Dynamics*, 15(4):976–984, July-August 1992.

[2] H. K. Khalil. *Nonlinear Systems*, volume Upper Saddle River, NJ. Prentice-Hall, second edition, 1996.

[3] S. Sastry. *Nonlinear Systems: Analysis, Stability, and Control*. Springer, New York, NY, 2013.

[4] N. Hovakimyan and C. Cao. L_1 *Adaptive Control Theory: Guaranteed Robustness with Fast Adaptation*. Society for Industrial and Applied Mathematics, Philadelphia, PA, 2010.

[5] M. Krstic, I. Kanellakopoulos, and P. V. Kokotovic. *Nonlinear and Adaptive Control Design*. Wiley, Hoboken, NJ, 1995.

[6] K. J. Åström and B. Wittenmark. *Adaptive Control*. Courier Corporation, North Chelmsford, MA, 2013.

[7] A. van der Schaft. *L2-Gain and Passivity Techniques in Nonlinear Control*, volume 2. Springer, 2000.

[8] R. Ortega and E. Garcia-Canseco. Interconnection and damping assignment passivity-based control: A survey. *European Journal of control*, 10(5):432–450, 2004.

[9] R. Ortega, A. van der Schaft, B. Maschke, and G. Escobar. Interconnection and damping assignment passivity-based control of port-controlled hamiltonian systems. *Automatica*, 38(4):585–596, 2002.

[10] Humberto Gonzalez, Manuel A Duarte-Mermoud, Ian Pelissier, Juan Carlos Travieso-Torres, and Romeo Ortega. A novel induction motor control scheme using ida-pbc. *Journal of Control Theory and Applications*, 6(1):59–68, 2008.

[11] José Ángel Acosta, MI Sanchez, and Aníbal Ollero. Robust control of underactuated aerial manipulators via ida-pbc. In *53rd IEEE Conference on Decision and Control*, pages 673–678. IEEE, 2014.

[12] ME Guerrero, DA Mercado, R Lozano, and CD García. Ida-pbc methodology for a quadrotor uav transporting a cable-suspended payload. In *2015 International Conference on Unmanned Aircraft Systems (ICUAS)*, pages 470–476. IEEE, 2015.

[13] Burak Yüksel, Cristian Secchi, Heinrich H Bülthoff, and Antonio Franchi. Reshaping the physical properties of a quadrotor through ida-pbc and its application to aerial physical interaction. In *2014 IEEE International Conference on Robotics and Automation (ICRA)*, pages 6258–6265. IEEE, 2014.

[14] Abeje Y Mersha, Raffaella Carloni, and Stefano Stramigioli. Port-based modeling and control of underactuated aerial vehicles. In *2011 IEEE International Conference on Robotics and Automation*, pages 14–19. IEEE, 2011.

[15] LE Muñoz, Omar Santos, Pedro Castillo, and Isabelle Fantoni. Energy-based nonlinear control for a quadrotor rotorcraft. In *2013 American Control Conference*, pages 1177–1182. IEEE, 2013.

[16] Burak Yüksel, Cristian Secchi, Heinrich H Bülthoff, and Antonio Franchi. Aerial physical interaction via ida-pbc. *The International Journal of Robotics Research*, 38(4):403–421, 2019.

[17] C. A. Woolsey. Cross-track control of a slender, underactuated auv using potential shaping. *Ocean Engineering*, 36(1):82–91, 2009.

[18] Jean-Michel W Fahmi and Craig A Woolsey. Directional stabilization of a fixed-wing aircraft using potential shaping. In *2018 Atmospheric Flight Mechanics Conference*, page 3620, 2018.

[19] Francis Valentinis, Alejandro Donaire, and Tristan Perez. Energy-based motion control of a slender hull unmanned underwater vehicle. *Ocean Engineering*, 104:604–616, 2015.

[20] Francis Valentinis, Alejandro Donaire, and Tristan Perez. Energy-based guidance of an underactuated unmanned underwater vehicle on a helical trajectory. *Control Engineering Practice*, 44:138–156, 2015.

[21] Francis Valentinis and Craig Woolsey. Nonlinear control of a subscale submarine in emergency ascent. *Ocean Engineering*, 171:646–662, 2019.

[22] J. M. Fahmi and C. A. Woolsey. Port-hamiltonian flight control of a fixed-wing aircraft. *IEEE Transactions on Control Systems Technology*, pages 1–8, 2021. DOI: 10.1109/TCST.2021.3059928.

[23] K. Fujimoto, K. Sakurama, and T. Sugie. Trajectory tracking control of port-controlled Hamiltonian systems via generalized canonical transformations. *Automatica*, 39(12):2059–2069, 2003. DOI: 10.1016/j.automatica.2003.07.005.

[24] B Etkin. *Dynamics of Atmospheric Flight*. Dover, Mineola, NY, 1972.

[25] CA Woolsey and L Techy. Cross-track control of a slender, underactuated auv using potential shaping. *Ocean Engineering*, 36(1):82–91, 2009.

[26] P Encarnacao and Antnio Pascoal. 3d path following for autonomous underwater vehicle. In *Proceedings of the 39th IEEE conference on decision and control (Cat. No. 00CH37187)*, volume 3, pages 2977–2982. IEEE, 2000.

[27] E Borhaug and Kristin Y Pettersen. Cross-track control for underactuated autonomous vehicles. In *Proceedings of the 44th IEEE Conference on Decision and Control*, pages 602–608. IEEE, 2005.

[28] James L Gresham, Jean-Michel W Fahmi, Benjamin M Simmons, Joseph W Foster, and Craig A Woolsey. Flight test approach for modeling and control law validation for unmanned aircraft. 2022.